Numerical Computation of the Interaction between Bluff Bodies in a Viscous Flow

AUTHOR(S):

Alam, Md.S.; Kuwamura, Tetuya; Kuwahara, Kunio; Takumi, Hideo

CITATION:

Alam, Md.S. ...[et al]. Numerical Computation of the Interaction between Bluff Bodies in a Viscous Flow. 数理解析研究所講究録 1983, 476: 125-143

ISSUE DATE:

1983-01

URL:

http://hdl.handle.net/2433/103317

数理解析研究所講究録
476巻 1983年 125-143

Numerical Computation of the Interaction between Bluff Bodies in a Viscous Flow

Md.S.Alam, Tetuya Kawamura, Kunio Kuwahara*, and Hideo Takami

Department of Applied Physics, The University of Tokyo, Tokyo,
*The Institute of Space and Astronautical Science, Tokyo

§1 Introduction

A large number of numerical investigations of the Navier-Stokes equations have been done, but flows past a number of bluff bodies remain relatively untouched mainly due to a lack of suitable coordinate systems. The purpose of this study is to develop a method applicable to solving problems of fluid flow with suspended particles or droplets arranged in rows or in random position, such as those seen in various engineering and physical sciences. One example is the ink-jet problem[1] where a liquid jet emanating from a nozzle breaks up into many droplets.

Great difficulty is encountered in solving these equations by the finite-difference method, that is, where there is no general coordinate system. In the case of square bodies, we can use rectangular meshes, as done by Matida et al[2]. In the case of curved bodies, however, the surface of the body does not necessarily coincide with meshes. This requires the values of the physical quantities on the surface be computed by interpolation. Since the gradient of these functions is very large there, we cannot expect to get accurate results by using such a coordinate system. We can also solve this problem by using a body fitted coordinate system (for example see Thames et al[3]). In this case, the Navier-Stokes equations become complicated; moreover, for problems in which bodies change their relative positions, extra computation time is needed to generate

coordinates fitted for a number of bodies at every time step.

To avoid the above difficulties, a new method called method of matching is developed. The idea of this method is that we subdivide the entire flow region into smaller regions, each of which surrounds only one body, and solve the governing equations for each region by using suitable coordinate system. To do so, we first take an overlap region between two adjacent ones and solve the equations for each region in such a way that the solutions within the overlap region coincide with each other. The chief advantage of this method is that, if a suitable coordinate system is found for a region surrounding each single body, one can solve the entire flow past a number of bodies by matching the solution in each subregion through the overlap region.

Using this method, a number of problems are solved: a) Flow past two square cylinders, b) Flow past two circular cylinders. c) Flow past two spheres. Problems c) is also solved under periodic boundary conditions. This provides a good model for the ink-jet problem.

§2 Steady Flow past Two Square Cylinders in a Channel

We consider the steady two-dimensional viscous flow past two square cylinders which are set perpendicular to a two-dimensional Poiseuille flow between two stationary parallel walls (Fig.1). This particular problem is studied for numerical test of our method. The bodies are placed both at off-center positions. In this case, we have to pay special attention to determining the values of stream function on the surface of the bodies.

Let the two bodies of equal size be set perpendicular to a Poiseuille flow in a channel of width 2 and the distances between the center axis of the bodies and the plane of symmetry of the channel be +s and -s. The motion of an incompressible viscous fluid is governed by the Navier-Stokes equations, which can be written in stream function-vorticity formulation as follows:

$$\Delta\psi + \omega = 0 \quad , \tag{2.1}$$

$$\Delta\omega + R\left(\frac{\partial\psi}{\partial x}\frac{\partial\omega}{\partial y} - \frac{\partial\psi}{\partial y}\frac{\partial\omega}{\partial x}\right) = 0 . \tag{2.2}$$

where R is the Reynolds number and Δ is the two-dimensional Laplacian.

The boundary conditions are

$$\left.\begin{aligned} \psi &\to y - \frac{y^3}{3} , \\ \omega &\to 2y \end{aligned}\right\} \quad \text{at} \quad x = \pm\infty , \tag{2.3}$$

$$\left.\begin{aligned} \psi &= \pm\frac{2}{3} , \\ \frac{\partial\psi}{\partial y} &= 0 \end{aligned}\right\} \quad \text{at} \quad y = 1 . \tag{2.4}$$

If s=0, the two bodies are both in symmetrical position and the constant values of the stream function on the surface of the bodies S_1 and S_2 are zero, but if $s\neq 0$, that is, the two bodies are in off-centered positions, ψ is subjected to the boundary condition

$$\begin{aligned} \psi &= \psi_{S_1} \quad \text{on } S_1 , \\ \psi &= \psi_{S_2} \quad \text{on } S_2 , \\ \frac{\partial\psi}{\partial n} &\quad \text{(normal derivative)} = 0 \quad \text{on } S_1 \text{ and } S_2 , \end{aligned} \tag{2.5}$$

where ψ_{S_1} and ψ_{S_2} are certain constants which must be determined based on the condition that the pressure be single-valued throughout the whole field[2]. This condition is expressed by

$$\oint_{C_1} dP = \oint_{C_2} dP = 0 , \tag{2.6}$$

where C_1 and C_2 are any closed paths enclosing each body. When applying the matching procedure, we need further boundary conditions on B C and B' C' (see Fig.1) which are obtained by solving the equations(2.1) and (2.2).

Initially, this problem was solved without using matching procedure. The domain used in numerical computation was finite and was divided into square meshes. The differential quotients

are approximated by three-point central-difference quotients. The solutions to the finite difference equations were obtained by successive iteration. The constants ψ_{S_1} and ψ_{S_2} were determined as the converged values of $\psi^m_{S_1}$ and $\psi^m_{S_2}$ as $m\to\infty$ according to

$$\psi^{m+1}_{S_1} = \psi^m_{S_1} + \lambda \sum_{C_1} \Delta P, \tag{2.7}$$

$$\psi^{m+1}_{S_2} = \psi^m_{S_2} + \lambda \sum_{C_2} \Delta P \tag{2.8}$$

where λ is a relaxation parameter. The sums $\sum_{C_1}\Delta p$ and $\sum_{C_2}\Delta p$ mean difference analogues to the integrals $\oint_{C_1} dp$ and $\oint_{C_2} dp$, where C_1 and C_2 are any rectangular paths PQRS and P'Q'R'S' enclosing the cylinders.

Now, in applying the matching procedure, the numerical calculations are first carried out for the front body in the region ABCD under the boundary conditions on BC which are, at first, those of Poiseuille flow. In this way, the values of ψ, ω on the line B'C' are obtained. Using these as the boundary values, the numerical computations are to be done for the rear body in the region A'B'C'D'. Then the boundary values on BC (for the front body) are improved, and, therefore, using these improved values, the calculations for the region ABCD are performed again. Such processes are repeated until the boundary values of ψ and ω on BC (therefore also on B'C') converge. The successive iteration are brought to an end when we get

$$|\psi^{n+1}_{i,j} - \psi^n_{i,j}| \leqq \varepsilon \quad \text{and} \quad |\omega^{n+1}_{i,j} - \omega^n_{i,j}| \leqq \varepsilon$$

for all i,j, where $\varepsilon = 10^{-6}$.

The upstream and downstream boundary on which the Poiseuille velocity profile is imposed were set at $X_- = -3.0$ and $X_+ = 3.0$. The mesh length h was taken to be equal to 1/10. The numerical computation was carried out for two different overlap regions -- one between 28th and 34th mesh lines and the other between 28th and 31st mesh lines. The side length of the bodies is fixed to be equal to 2/5. The front body is set at a streamwise distance 1.4 from O and the rear body is set at 3.9 from O. The other parameters are R = 20, d = 0.2, λ = 0.001 and n (nummbers of

iteration per one matching procedure) = 1 and 100.

Fig.2 shows (a) streamlines and (b) equivorticity lines. The following four cases are studied:

Case 1: Without matching procedure.

Case 2: The overlap region was taken between 28th and 34th mesh lines and the process of matching was done at every iteration, i.e., n=1.

Case 3: Same as the Case 2, but n=100.

Case 4: A narrower overlap region was taken (i.e., 28th-31st mesh lines), n=100.

All four cases gave exactly the same final results, but the efficiencies are very different. Case 3 was found to be the best of the above four cases, even better than Case 1. In Case 2, the values of ψ and ω were found to be oscillating in the initial stages (for 50 or 60 iterations), and it took much computation time to reach a converged solution. In Case 4, the narrower overlap region makes the values on the boundary lines BC and B'C' affect each other more strongly, thus worsening the rate of convergence of the iteration. If we take too wide an overlap region, the computation time becomes longer due to the large number of mesh points for each region surrounding the body.

From the above results, we can conclude that good results can be obtained by the matching procedure, that matching through overlap region should be performed after getting somewhat stable values for each region, and that overlap region should neither be too narrow nor too wide in order to minimize the computation time.

§3 Unsteady Flow past Two Circular Cylinders

Let us consider the unsteady flow of viscous fluid past two circular cylinders of the same radius 1. At time t=0 the fluid is supposed to be set in motion impulsively with a constant velocity U in the direction of the positive x-axis. In polar coordinate (r,θ), the equations of motion can be written in the nondimensional form as

$$\frac{\partial \omega}{\partial t} - \frac{1}{r}\left(\frac{\partial \psi}{\partial r}\frac{\partial \omega}{\partial \theta} - \frac{\partial \psi}{\partial \theta}\frac{\partial \omega}{\partial r}\right) = \frac{2}{R}\Delta\omega \ , \qquad (3.1)$$

where $R=\frac{2U}{\nu}$ and $\Delta = \partial^2/\partial r^2 + (1/r)\partial/\partial r + (1/r^2)\partial^2/\partial\theta^2$. Functions ψ, ω and $\mathbf{v}=(v_r, v_\theta)$ are connected by

$$\omega = -\Delta\psi , \tag{3.2}$$

$$v_r = \frac{1}{r}\frac{\partial\psi}{\partial\theta} , \quad v_\theta = -\frac{\partial\psi}{\partial r} . \tag{3.3}$$

For the convenience of numerical computation, we introduce the disturbance stream function φ as

$$\psi = r\sin\theta + \varphi , \tag{3.4}$$

in which the first term of the right-hand side is due to the uniform flow.

The radial coordinate is transformed as follows:

$$\xi = \log r . \tag{3.5}$$

Using (3.4) and (3.5), the equations (3.1) and (3.2) become

$$e^{2\xi}\frac{\partial\omega}{\partial t} - \left(\frac{\partial\varphi}{\partial\xi}\frac{\partial\omega}{\partial\theta} - \frac{\partial\varphi}{\partial\theta}\frac{\partial\omega}{\partial\xi}\right) - e^{\xi}\left(\frac{\partial\omega}{\partial\theta}\sin\theta - \frac{\partial\omega}{\partial\xi}\cos\theta\right) - \frac{2}{R}\Delta\omega = 0, \tag{3.6}$$

$$\omega = -e^{-2\xi}\Delta\varphi , \tag{3.7}$$

where

$$\Delta = \frac{\partial^2}{\partial\xi^2} + \frac{\partial^2}{\partial\theta^2} . \tag{3.8}$$

We solve the equations (3.6) and (3.7) under the following initial and boundary conditions. The initial condition is that of uniform flow, and the boundary conditions used are

1) $\varphi = 0, \omega = 0$ along the centerline, and at $\pm\infty$. (3.9)

2) $\varphi = \sin\theta, \frac{\partial\varphi}{\partial\xi} = -\sin\theta$ at $\xi = 0$. (3.10)

Since it is difficult to treat the problem in an infinite domain, we restrict the computational domain within circles of sufficiently large radius r_∞ ($=\exp\Xi$) in physical plane. As the

flow is assumed to be symmetric with respect to the lines $\theta=0$ and $\theta=\pi$, only the upper half of the flow region need be considered. Actually, the numerical computations are carried out for the domain ABCDA for the front body O and A'B'C'D'A' for the rear body O' (see Fig.3 (a)); the overlap region is DD'C'ED. Thus in the transformed plane, i.e., in (ξ,θ) plane, the regions of computation reduce to ABCDEA and A'B'C'D'E'A' (Fig.3 (b)).

Three -point central difference for the space derivatives and forward difference for the time derivative are used. We take mesh constant $\Delta\xi=\Delta\theta=\frac{\pi}{40}$, and take $\xi=\pi$ ($r_\infty=\exp\pi=23.1407$).

At first, the flow for region I is solved according to the following steps:

1) At t=0, take $\psi=0$ and $\omega=0$ at all mesh points except on the surface of cylinder O, where $\psi=-\sin\theta$ and $\omega=0$.

2) Solve eq.(3.7) for ψ, by successive overrelaxation method.

3) Calculate the boundary values of ψ and ω on zigzag lines for region II (for rear body) by linear interpolation from the values of ψ and ω already obtained in front flow region.

Next, the flow for region II is solved according to the repetition of steps 1) - 3) and using the calculated boundary values of 3) on zigzag lines D'C'.

4) Compute new boundary values of ψ and ω on zigzag lines for region I (for front body) in a similar way as described in step 3).

In order to match the two flows within the overlap region, steps 2) to 4) are repeated until a sufficient convergence is obtained.

5) Calculate the vorticity ω on the surface of the bodies by using eq.(3.6).

6) Calculate the vorticity at $t=\Delta t$ using eq.(3.6) for regions I and II, and go back to 2) for next time step.

The computing time steps Δt must be restricted to ensure numerical stability. The criteria used[4] is

$$\frac{2\Delta t}{e^{2\xi} R (\Delta \xi)^2} < \frac{1}{4} . \qquad (3.11)$$

In view of this criterion, the time steps were taken as $\Delta t=0.005$ for R=10 and $\Delta t=0.025$ for R=40 and 100.

Numerical computation was carried out for the cases shown in Table 1, where d is the distance between the centers of the two circular cylinders. The computed drag coefficients are summarized in this Table, where C_{D_p}, C_{D_f} and C_D are pressure, frictional and total drag coefficients respectively.

Figs.4, 5, 6 and 7 show streamlines and equivorticity lines for R=40 at nondimensional time t=24 and d is equal to 10 and 6. The overlap region is approximately between two dotted lines, the boundary lines are taken just outside of these dotted lines. In Fig.8, C_D is plotted against d for various values of R. In Fig.9, C_D is plotted against R for various values of d. In case of low Reynolds numbers, the interaction between the bodies fade away rapidly when they are placed at large distance. In case of large Reynolds numbers, the interaction is large even when the bodies are placed at large distance. A negative value for drag coefficient C_D appears in some cases, which indicates that if two bodies are let to move freely, the rear body moves toward the front body againt direction of flow.

The rate of convergence was found to be small for low Reynolds numbers or for narrow overlap region, but large for large Reynolds numbers. At low Reynolds numbers, viscous effects are predominant in the flow field; this means values of ψ and ω on the downstream boundary of the overlap region strongly affect those on the upstream boundary because of viscous dissipation. Also, when the overlap region is narrow, the improved but unstable boundary values affect each other strongly. This interaction between the two boundaries of the overlap region causes the slow rate of convergence. For large Reynolds numbers, convection terms are predominant and values on down-stream boundary of the overlap region do not affect strongly those on the up-stream boundary. This is the reason of good convergence at large Reynolds numbers.

The above results show that the present method is effective

even if one must have recourse to interpolation in the process of matching.

§4 Unsteady Axisymmetrical Flow past Two Spheres

Let us consider the unsteady three-dimensional axisymmetric flow past two spheres of the same radius 1. Let (r,θ,ϕ) be the spherical polar coordinates. We shall assume the axial symmetry: $\frac{\partial}{\partial\phi}=0$ and $V_\phi=0$. The vorticity equation can be written in terms of the spherical polar coordinates in conservation form:

$$\frac{\partial\omega}{\partial t}+\frac{\partial}{\partial r}(\omega V_r)+\frac{1}{r}\frac{\partial}{\partial\theta}(\omega V_\theta)+\frac{\omega V_r}{r}$$
$$=\frac{2}{R}\left(\frac{\partial^2\omega}{\partial r^2}+\frac{1}{r^2}\frac{\partial^2\omega}{\partial\theta^2}+\frac{2}{r}\frac{\partial\omega}{\partial r}+\frac{1}{r^2}\cot\theta\frac{\partial\omega}{\partial\theta}-\frac{\omega}{r^2\sin^2\theta}\right), \tag{4.1}$$

where R is the Reynolds number based on sphere diameter: $R=2U/\nu$ (U is the velocity of uniform flow at infinity). The vorticity has only the ϕ-component and is connected by Stokes stream function ψ as follows :

$$V_\theta=-\frac{1}{r\sin\theta}\frac{\partial\psi}{\partial r}, \qquad V_r=\frac{1}{r^2\sin\theta}\frac{\partial\psi}{\partial\theta}, \tag{4.2}$$

$$\omega=-\frac{1}{r\sin\theta}\left[\frac{\partial^2}{\partial r^2}+\frac{\sin\theta}{r^2}\frac{\partial}{\partial\theta}\left(\frac{1}{\sin\theta}\frac{\partial}{\partial\theta}\right)\right]\psi. \tag{4.3}$$

In order to solve (4.1) and (4.3), we take the same type of transformation as in the case of circular cylinder:

$$\xi=\log r, \tag{4.4}$$

$$\psi=\frac{1}{2}r^2\sin^2\theta+\varphi, \tag{4.5}$$

where φ is the disturbance stream function.

The boundary conditions are taken to be similar to the cylindrical problems. The numerical computations are carried out in exactly the same way as in the problem of circular cylinders. The convergence criteria, step size and Reynolds numbers are the same.

Figs.10-13 show the flow patterns at Reynolds number 40. Drag coefficients calculated by our methods are listed in Table 2. In Fig.14, the total drag coefficient C_D is plotted against d. In Fig.15, C_D is plotted against R for various values of d. For all Reynolds numbers, the front and the rear bodies have decreasing values of C_D when the two bodies are placed closer. The change of C_D versus d for low Reynolds number is especially large for the rear body as in the two-dimensional case. When the spheres are separated far away from each other, there is little interaction between them for low Reynolds number, but in the case of high Reynolds numbers some interaction remains.

We shall now compare the results for spheres with those for circular cylinders. The trend of elongation of vorticity and wake region in downstream direction is much smaller for spheres than for cylinders. In spherical problems, the frictional force is greater than the pressure force. The difference is larger at lower Reynolds number whereas their ratio decreases with an increase in Reynolds numbers. On the contrary, in cylindrical problem, we find that the pressure force is larger than the frictional force and their difference increases with increasing Reynolds numbers.

§5 Flows past Spheres Periodically Arranged in a Row

In the preceding chapters, the method of matching was applied to flows past two bodies. This method can be used in principle to compute flows past any number of bodies; the only problem is large computing time necessary for convergence owing to the increase of the number of subdomains in which the solutions are to be matched with each other. However, when the bodies are arranged periodically in the streamwise direction, it is not difficult to compute the field if one replaces one of the matching conditions by that of periodicity. In this way one can analyze the flow problems which are important in engineering science, e.g., unsteady flow past infinitely many spheres periodically arranged in a line -- a realistic model of a row of small spherical drops appearing in an ink jet.

In this section, flows past a row of spheres are computed, where periodic boundary conditions are imposed. Keeping the ink-jet phenomenon in mind, we carried out numerical computation for the following three cases (see Fig.16).

1) Spheres of different sizes are placed at equal intervals (d=8.25).

2) The larger sphere is at a distance 5.5 in front of the smaller one.

3) The smaller sphere is at a distance 5.5 in front of the larger one.

In all these cases, the radius of the larger sphere is 2.5 times larger than that of the smaller one. Reynolds number, based on the diameter of the larger sphere, is 75 in all the cases. This Reynolds number is within the range where the droplet formation of two different sizes were observed in an ink jet[1]. The other parameters are taken to be the same as in the previous case.

The flow patterns are shown in Figs.17-18 for Case 1, in Figs.19-20 for Case 2 and in Figs.21-22 for Case 3. Figs.23-25 show the changes of drag coefficients C_D, C_{D_p}, C_{D_f} and instantaneous accelaration C_D/a^* of the two bodies. The experimental results due to Chaudhary et al. are cited in Fig.26 for the sake of comparison. In Case 1, the instantaneous acceleration is almost the same for both bodies after some time, and the two bodies will not change their relative positions if set in free motion (see also Fig.26(a)). In Case 2, the rear body enters the wake of the front body and the acceleration is retarded by the influence of the wake of the front body. Due to the larger acceleration, the front body will merge rapidly with the rear body (see also Fig.26(f)). In Case 3, the larger rear body enters the wake region of the front body, and both are influenced by each other (see also Fig.26(i)). Due to greater acceleration of the front body, it may approach the rear body, but it will take longer time to merge with the rear body. Thus, the experimental results are well-confirmed qualitatively.

---

*If the sphere of radius a is set free at some instant, it will begin to move with the acceleration proportional to C_D/a.

§6 Conclusion

The method of matching has been developed for the numerical solution of the finite-difference form of the Navier-Stokes equations for unsteady flows past a number of bluff bodies. The essential feature of this method is that if one can find a suitable coordinate system for solving the equations for each region around a single body, it is possible to solve them for the entire region surrounding a number of bodies irrespective of shape and size , by matching individual single-body solutions through overlap regions. Computational time for numerical solutions of two-body problems by this method is not much longer than twice that for a single-body problem, especially at higher Reynolds numbers where inertia terms predominate and the change of state occurring at a point in the fluid is transmitted mainly in the downstream direction.

Using this method, we solved a number of flow problems, i.e., a) flow past two square cylinders, b) flow past two circular cylinders and c) flow past two spheres. The numerical calculations have also been carried out for flow past spheres arranged periodically in a row. The results of the sphere problems provided a good qualitative confirmation of the work of Chaudhary et al.

REFERENCES

1) Chaudhary, K.C. and Maxworthy, T., The nonlinear capillary instability of liquid jet, Part 3: Experiments on satellite drop formation and control. J. Fluid Mech. 96, 287 (1980).
2) Matida, Y., Kuwahara, K., and Takami, H., Numerical study of a steady two-dimensional flow past a square cylinder in a channel. J. Phys. Soc. Jpn. 38, 1522 (1975).
3) Thames, F.C., Thompson, J.F., Mastin, C.W., and Walker, R.L., Numerical solution for viscous and potential flow about arbitrary two-dimensional bodies using body fitted coordinate systems. J. Comput. Phys. 24, 245(1977).
4) Kawaguti, M. and Jain, P., Numerical study of a viscous fluid flow past a circular cylinder. J. Phys. Soc. Jpn. 21, 2055(1966).

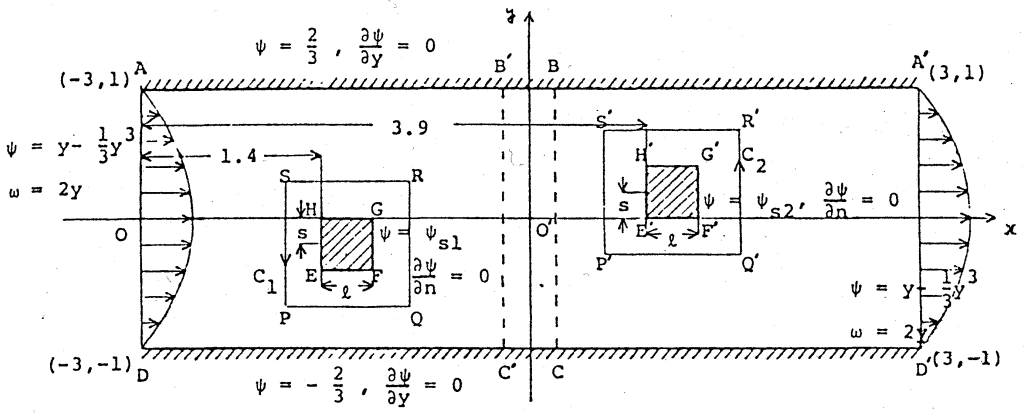

Fig. 1. Two-dimensional steady flow past two square cylinders.

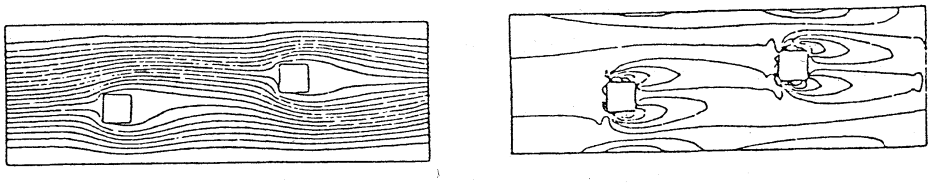

Fig. 2. (a) streamlines, (b) equi-vorticity lines for $R = 20$ (two square cylinders).

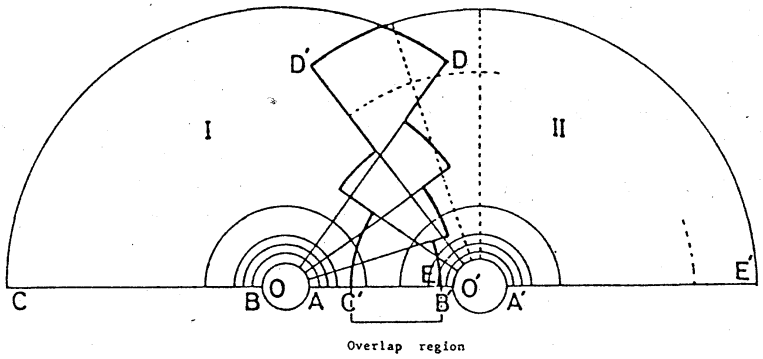

Fig. 3. (a) Geometry of bodies and meshes in physical plane.

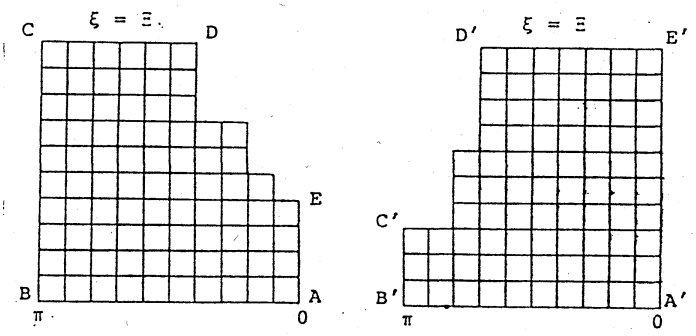

Fig. 3. (b) Geometry of meshes in transformed plane.

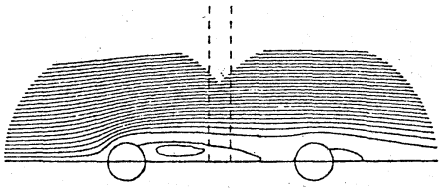

Fig. 4. Streamlines for $R = 40$, $d = 10$, $t = 24$ (two circular cylinders).

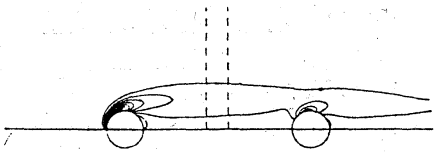

Fig. 5. Equi-vorticity lines for $R = 40$, $d = 10$, $t = 24$ (two circular cylinders).

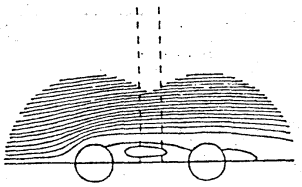

Fig. 6. Streamlines for $R = 40$, $d = 6$, $t = 24$ (two circular cylinders).

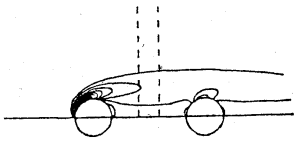

Fig. 7. Equi-vorticity lines for $R = 40$, $d = 6$, $t = 24$ (two circular cylinders).

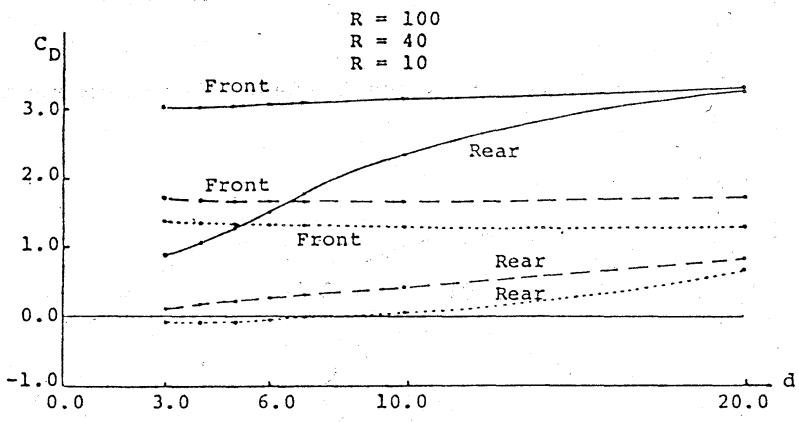

Fig. 8. C_D versus d for various R (two circular cylinders)

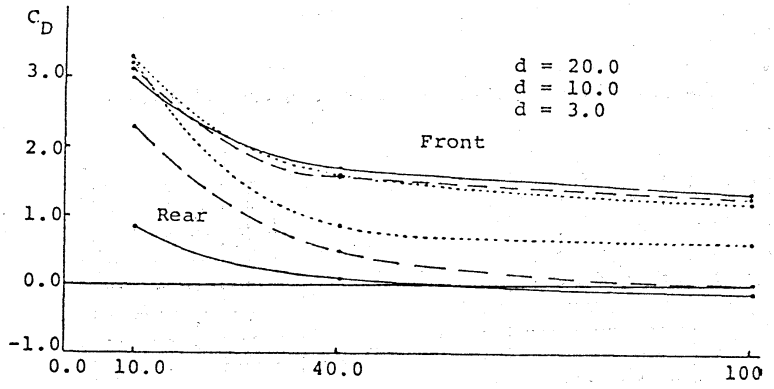

Fig. 9. C_D versus R for various d (two circular cylinders).

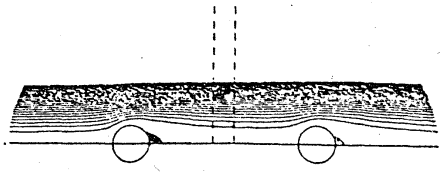

Fig. 10. Streamlines for $R = 40$, $d = 10$, $t = 24$ (two spheres).

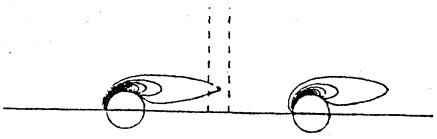

Fig. 11. Equi-vorticity lines for $R = 40$, $d = 10$, $t = 24$ (two spheres).

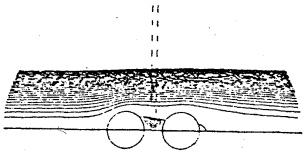

Fig. 12. Streamlines for $R = 40$, $d = 3$, $t = 24$ (two spheres).

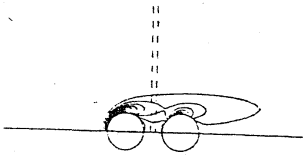

Fig. 13. Equi-vorticity lines for $R = 40$, $d = 3$, $t = 24$ (two spheres).

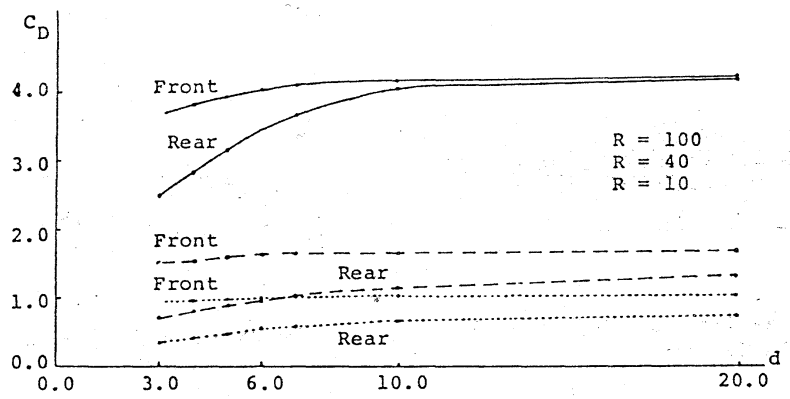

Fig. 14. C_D versus d for various R (two spheres).

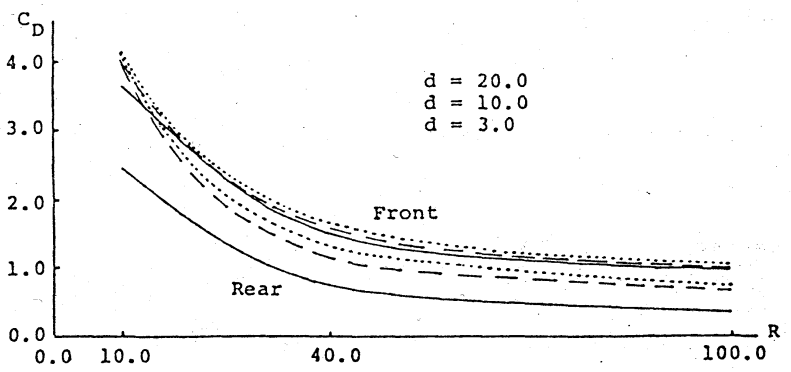

Fig. 15. C_D versus R for various d (two spheres).

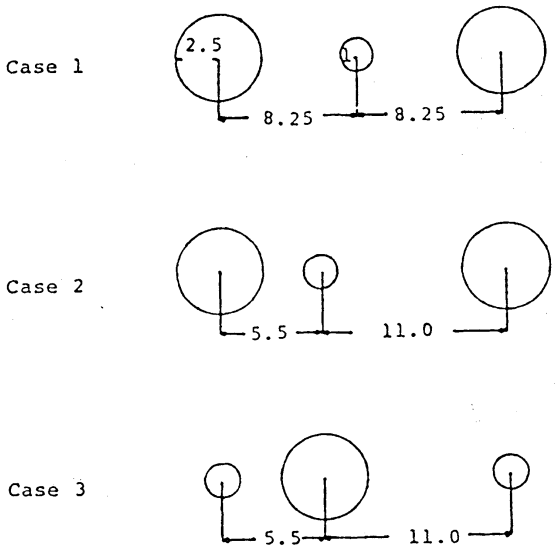

Fig. 16. Two spheres of unequal size placed periodically in three cases.

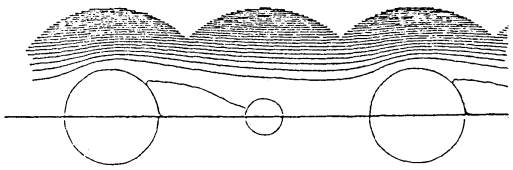

Fig. 17. Streamlines for $R = 75$, $t = 24$ in Case 1.

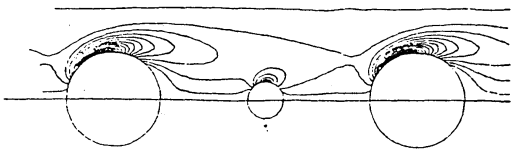

Fig. 18. Equi-vorticity lines for $R = 75$, $t = 24$ in Case 1.

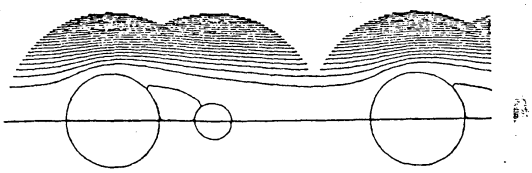

Fig. 19. Streamlines for $R = 75$, $t = 24$ in Case 2.

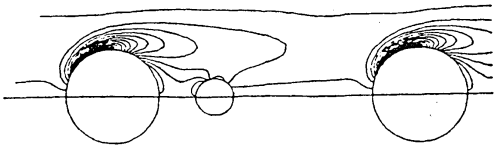

Fig. 20. Equi-vorticity lines for $R = 75$, $t = 24$ in Case 2.

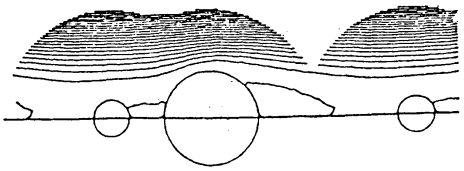

Fig. 21. Streamlines for $R = 75$, $t = 24$ in Case 3.

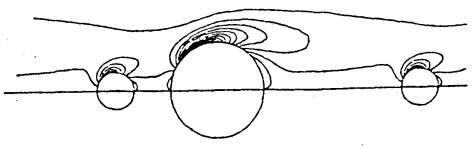

Fig. 22. Equi-vorticity lines for $R = 75$, $t = 24$ in Case 3.

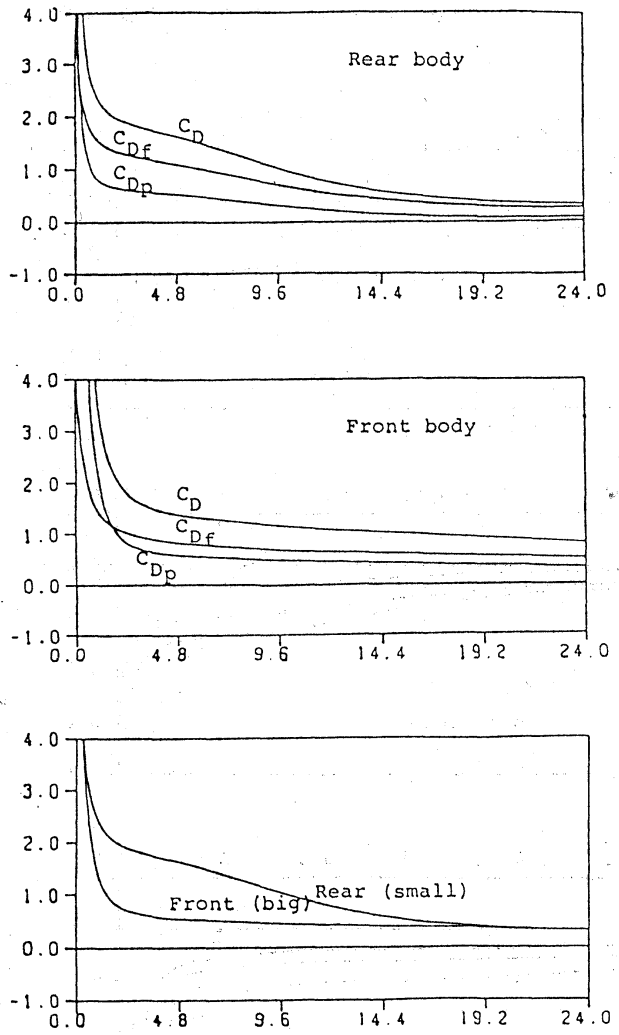

Fig. 23. Changes of drag coefficients and instantaneous acceleration for Case 1.

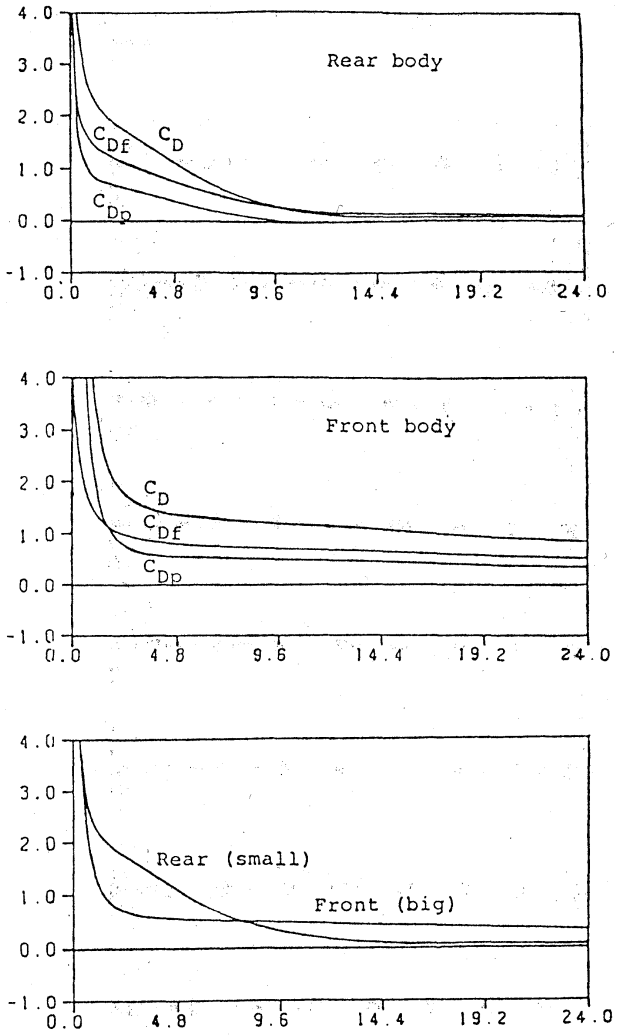

Fig. 24. Changes of drag coefficients and instantaneous acceleration for Case 2.

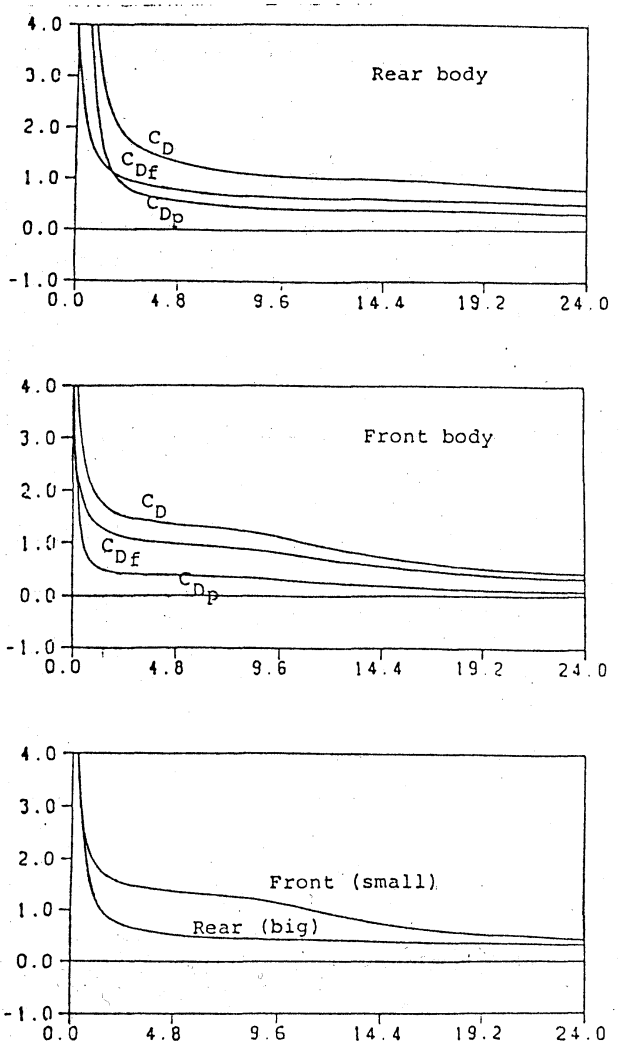

Fig. 25. Changes of drag coefficients and instantaneous acceleration for Case 3.

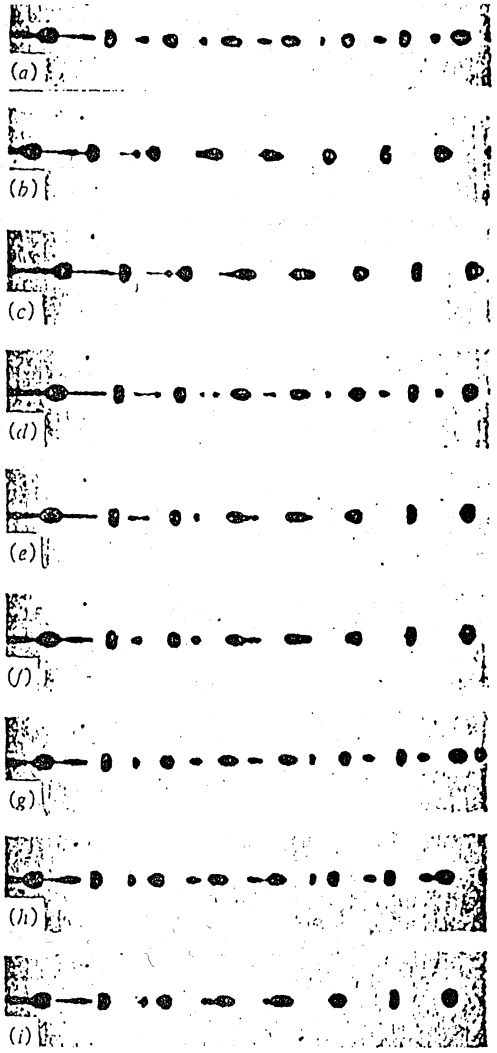

Fig. 26. Experimental works by Chaudhary *et al.*

Table 1

Reynolds number	d	Front cylinder C_{Dp}	C_{Df}	C_D	Rear cylinder C_{Dp}	C_{Df}	C_D
	3.0	1.745	1.274	3.019	0.318	0.557	0.875
	4.0	1.740	1.274	3.014	0.438	0.602	1.040
	5.0	1.751	1.281	3.032	0.560	0.705	1.265
10.0	6.0	1.756	1.287	3.043	0.728	0.754	1.482
	7.0	1.772	1.300	3.072	0.912	0.861	1.773
	10.0	1.797	1.316	3.113	1.266	1.043	2.309
	20.0	1.903	1.378	3.281	1.868	1.361	3.229
	3.0	1.158	0.540	1.698	−0.007	0.125	0.124
	4.0	1.145	0.533	1.678	0.040	0.128	0.168
	5.0	1.138	0.530	1.668	0.083	0.136	0.219
40.0	6.0	1.130	0.528	1.658	0.118	0.144	0.262
	7.0	1.128	0.527	1.655	0.155	0.154	0.309
	10.0	1.132	0.529	1.661	0.260	0.188	0.448
	20.0	1.150	0.535	1.685	0.535	0.322	0.857
	3.0	1.042	0.316	1.358	−0.126	0.029	−0.097
	4.0	1.028	0.312	1.340	−0.116	0.028	−0.088
	5.0	1.013	0.308	1.321	−0.105	0.027	−0.078
100.0	6.0	1.005	0.306	1.311	−0.062	0.036	−0.026
	7.0	0.992	0.303	1.295	−0.055	0.036	−0.019
	10.0	0.966	0.299	1.265	−0.003	0.040	0.037
	20.0	0.943	0.287	1.230	0.474	0.181	0.655

Table 2

Reynolds number	d	Front sphere C_{Dp}	C_{Df}	C_D	Rear sphere C_{Dp}	C_{Df}	C_D
	3	1.074	2.572	3.646	0.684	1.787	2.471
	4	1.141	2.657	3.798	0.824	1.991	2.815
	5	1.219	2.700	3.919	0.989	2.150	3.139
10	6	1.237	2.753	3.990	1.102	2.319	3.421
	7	1.248	2.805	4.053	1.125	2.538	3.663
	10	1.284	2.836	4.120	1.221	2.799	4.020
	20	1 294	2.869	4.163	1.291	2.867	4.158
	3	0.530	0.987	1.517	0.261	0.469	0.730
	4	0.540	0.999	1.539	0.274	0.564	0.838
	5	0.559	1.018	1.577	0.312	0.608	0.920
40	6	0.579	1.025	1.604	0.335	0.647	0.982
	7	0.583	1.104	1.623	0.355	0.672	1.027
	10	0.602	1.051	1.653	0.450	0.705	1.155
	20	0.605	1.061	1.666	0.464	0.844	1.308
	3	0.410	0.540	0.950	0.137	0.215	0.352
	4	0.410	0.541	0.951	0.163	0.262	0.425
	5	0.418	0.547	0.965	0.196	0.285	0.481
100	6	0.439	0.549	0.988	0.230	0.311	0.541
	7	0.440	0.562	1.002	0.234	0.327	0.561
	10	0.455	0.596	1.024	0.278	0.381	0.659
	20	0.456	0.574	1.030	0.312	0.420	0.732